Supporting Information for: The 2015–2017 Pamir Earthquake Sequence: Fore-, Main-, and Aftershocks, Seismotectonics and Fault Interaction

Wasja Bloch[1], Sabrina Metzger[1], Bernd Schurr[1], Xiaohui Yuan[1], Lothar Ratschbacher[2], Sanaa Reuter[2], Qiang Xu[3,4], Junmeng Zhao[3,4], Shokhruhk Murodkulov[5], Ilhomjon Oimuhammadzoda[6]

[1]GFZ German Research Centre for Geosciences, 14473 Potsdam, Germany

[2]Geologie, Technische Universität Bergakademie Freiberg, 09599 Freiberg, Germany

[3]Key Laboratory of Continental Collision and Plateau Uplift, Institute of Tibetan Plateau Research, Chinese Academy of Sciences, Beijing 100101, China

[4]CAS Center for Excellence in Tibetan Plateau Earth Sciences, Beijing 100101, China

[5]Institute of Geology, Earthquake Engineering and Seismology, Academy of Sciences, Dushanbe, Tajikistan

[6]Department of Geology under the Government of the Republic of Tajikistan, Dushanbe, Tajikistan

Contents of this file

Corresponding author: Wasja Bloch, wbloch@eoas.ubc.ca now at: Department of Earth, Ocean and Atmospheric Sciences, University of British Columbia, Vancouver, Canada.

Additional Supporting Information (Files uploaded separately)

1. Earthquake catalog
2. Moment tensor catalog

Introduction This supporting information contains the earthquake catalog and the focal mechanism catalog presented in the main body of the text, and additional figures. Please refer to to the Method's section for processing details.

Earthquake Catalog

seismic_event_catalog.txt

The seismic event catalog presented in the main article.

Columns are:

- Year, Month, Day, Hour, Minute, Second: Time of the seismic event
- Timestamp: Time of the event in seconds since 1. January 1970 (UTC)
- Longitude, Latitude: Coordinates of the event location in degree
- Depth: Depth of the event in kilometer
- P-picks, S-picks: Number of P- and S-wave arrival times used for event location
- revised?: 0 for not manually revised , 1 for revised arrival times
- method: Localization algorithm that yielded the reported location
- RMS: root-mean-square misfit of the *simulps* localization
- Magnitude, uncert: Magnitude of the seismic event and magnitude uncertainty
- type: Magnitude type. M_W moment magnitude; M_L calibrated local magnitude; NEIC moment magnitude published by NEIC.
- Sequence: Letter of the earthquake sequences discussed in the text. A-I: see main text. Z: Below 50 km depth. O: All other events

Moment Tensor Catalog

moment_tensor_catalog.txt

The moment tensor catalog presented in the main article.

Columns are:

1. Date (YYYY/MM/DD),

2. Time (hh:mm:ss),

3. Longitude (degree),

4. Latitude (degree),

5. Centroid depth (km),

6. Moment magnitude of the event

7. up-up,

8. south-south,

9. east-east,

10. up-south,

11. up-east,

12. south-east elements (10ˆexponent dyne·cm) of the moment tensor (Harvard convention)

13. exponent

14. Strike (degree)

15. Dip (degree)

16. Rake (degree) of the preferred focal mechanism

References

Utsu, T., Ogata, Y., et al. (1995). The centenary of the Omori formula for a decay law of aftershock activity. *Journal of Physics of the Earth*, *43*(1), 1–33.

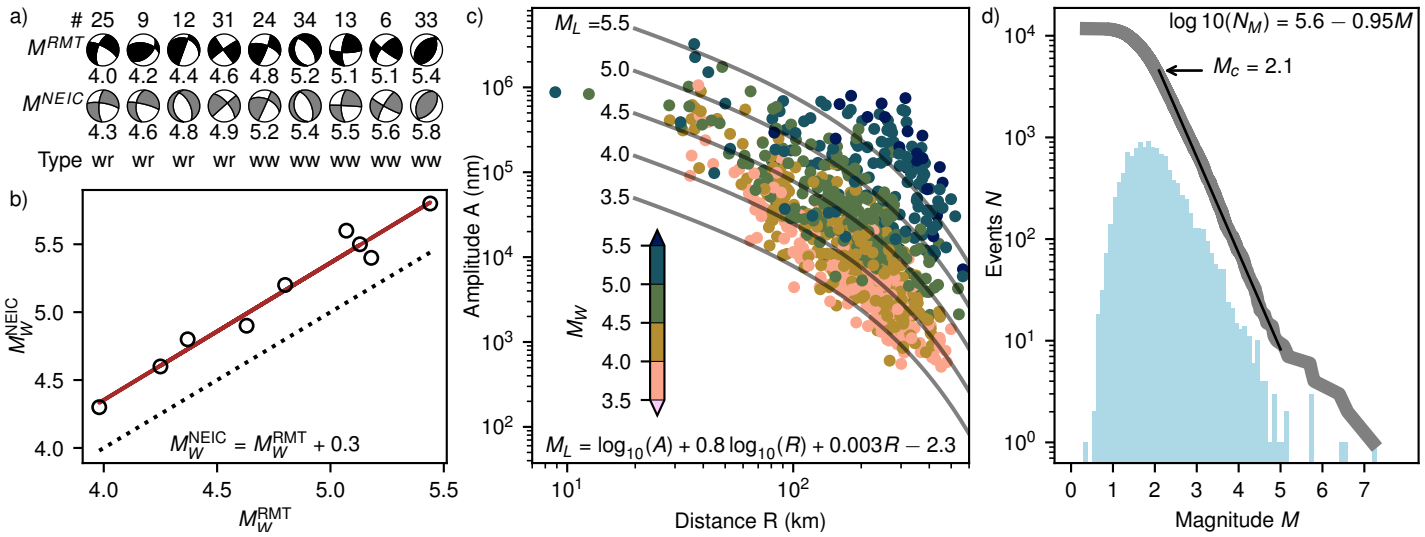

Figure S1. Moment magnitudes of seismic events. (a) and (b) Comparison of regional moment tensors (a) and magnitudes (b) with results by NEIC. (wr) regional (ww) W-phase. (c) Calibration of local magnitudes with parameters of Equation 1 of the main text. (d) Magnitude distribution of the entire catalog. (M_c) completeness magnitude.

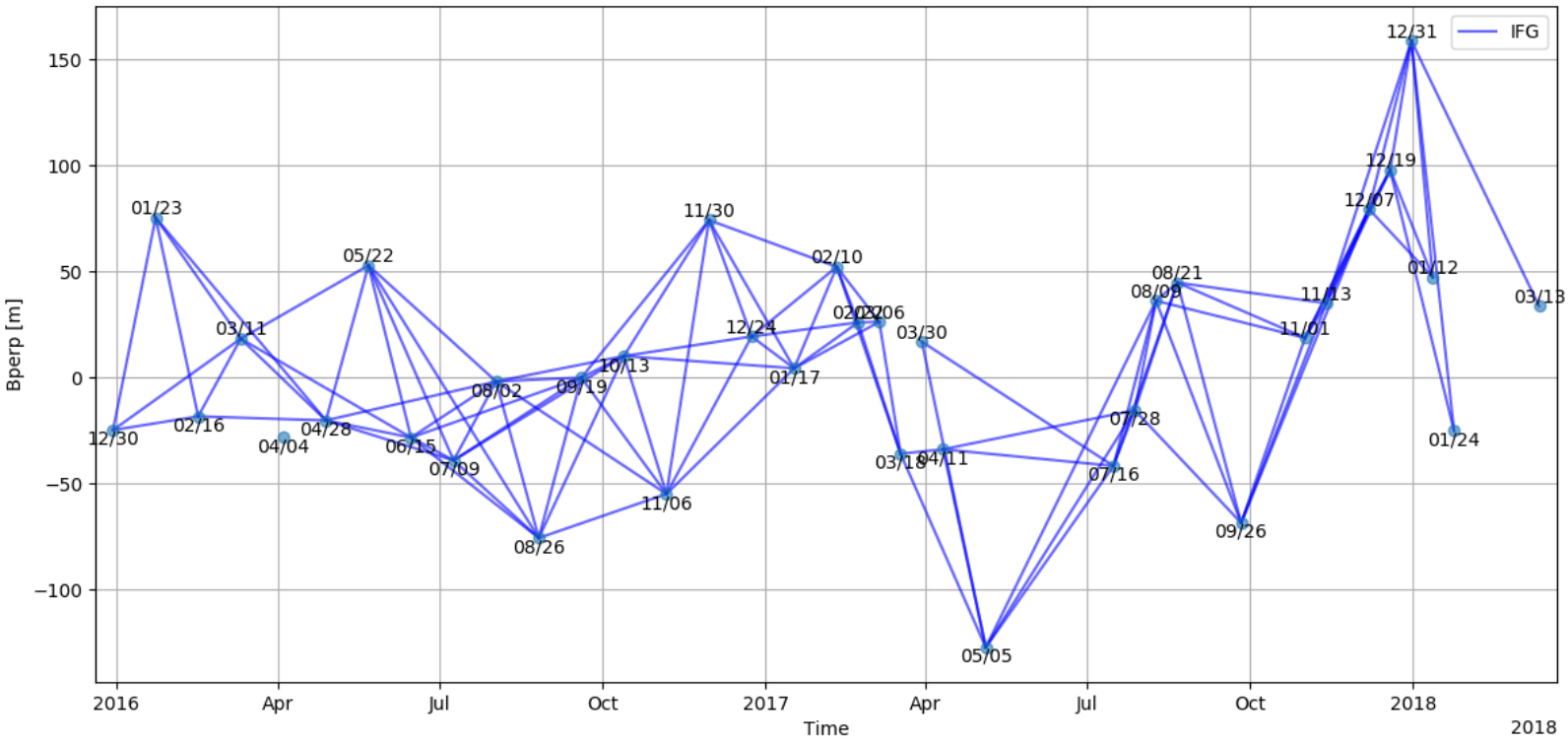

Figure S2. Perpendicular baseline (Bperp) against time for InSAR frame 100A_052 (Figures 4 and S5). Lines indicate combination of acquired images to compute differential interferograms.

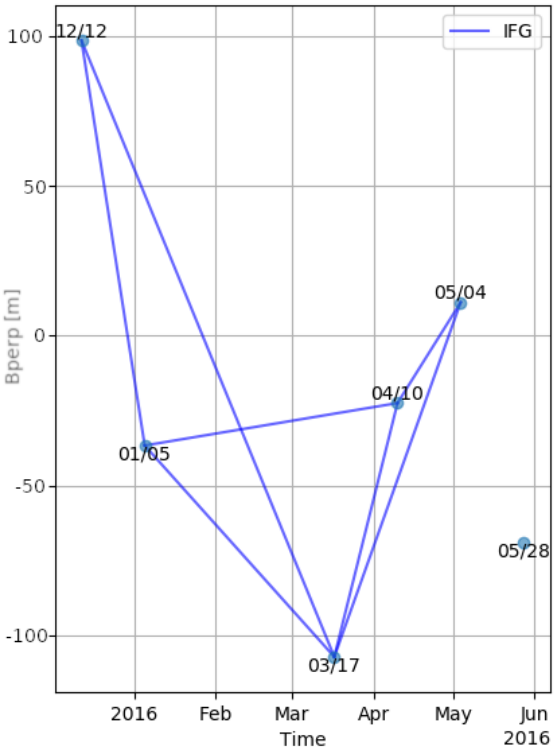

Figure S3. As Figure S2, but for frame 005D_050.

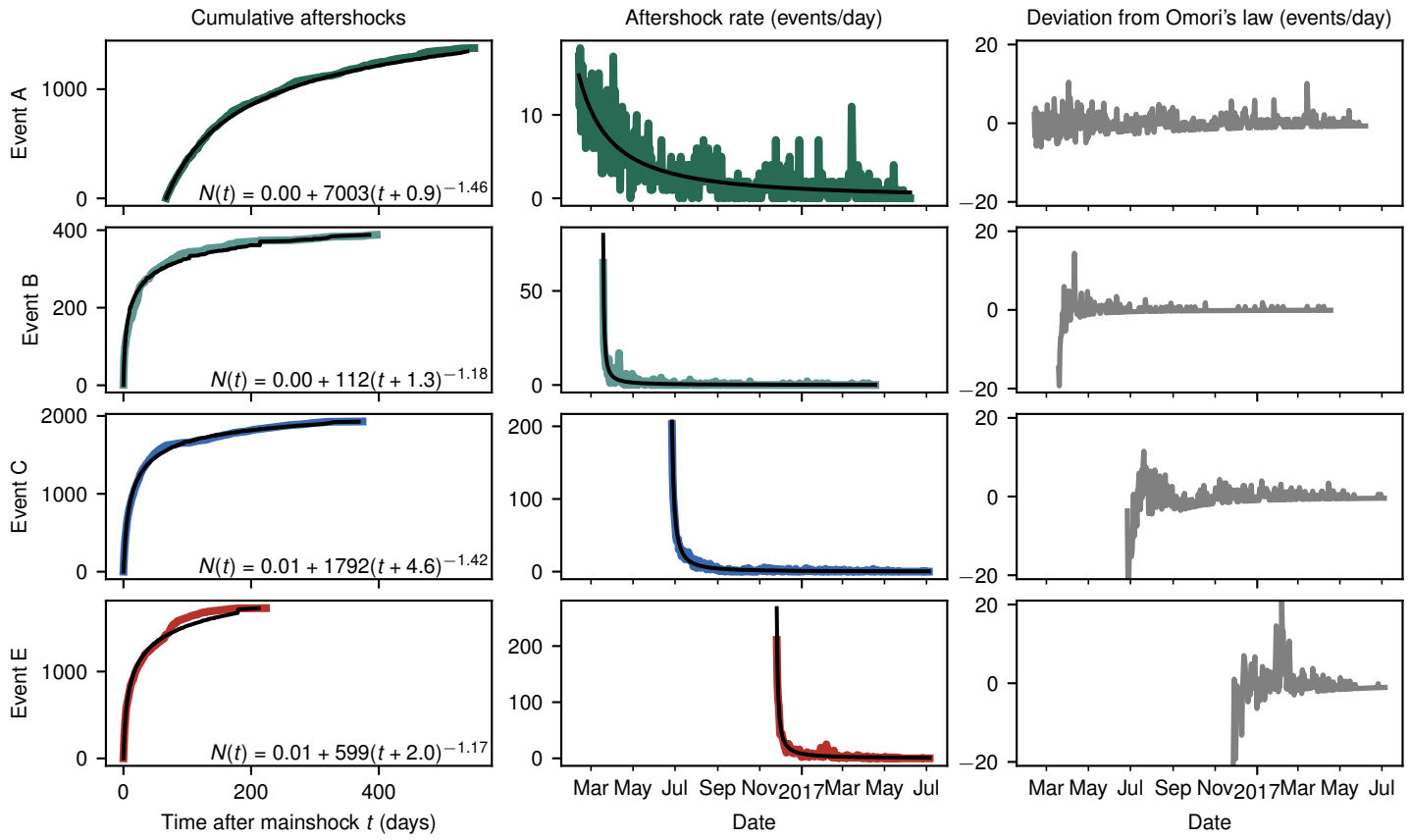

Figure S4. Aftershock characteristics of mainshock vicinities *A*, *B*, *C*, and *E*. Left column: Cumulative aftershocks after the mainshock (*A** only shown after installation of 8H network) and parameters of modified Omori's Law (Utsu et al., 1995). Middle column: Aftershock rate over time. Right column: Deviation of aftershock rate from Omori's law over Time. Even though time intervals of increased aftershock activity exist, they to not correlate with each other in between earthquake sequences.

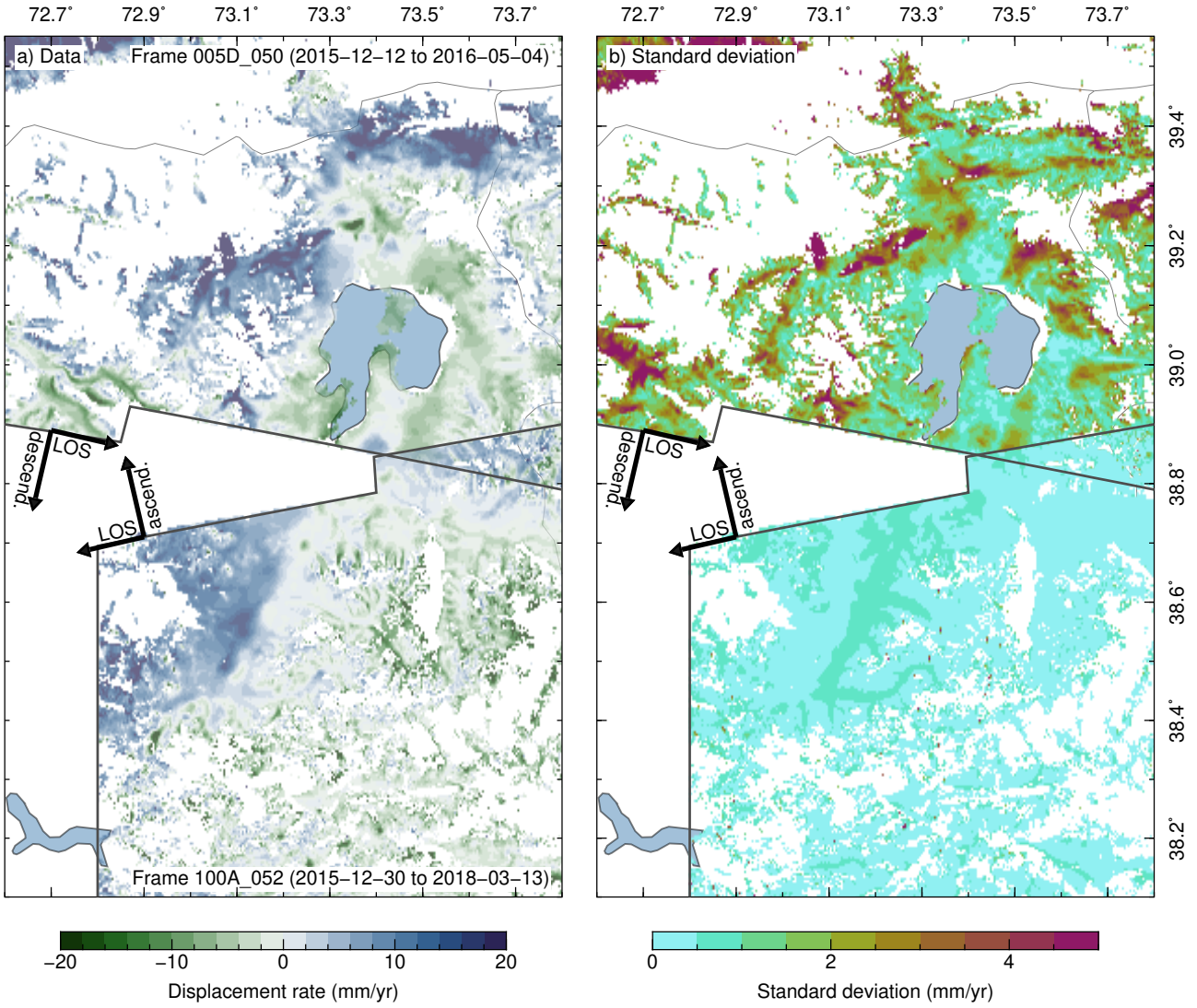

Figure S5. InSAR time series as in Figure 4. Left: rate map before conversion to displacement. Right: Nominal uncertainty of displacement rate.

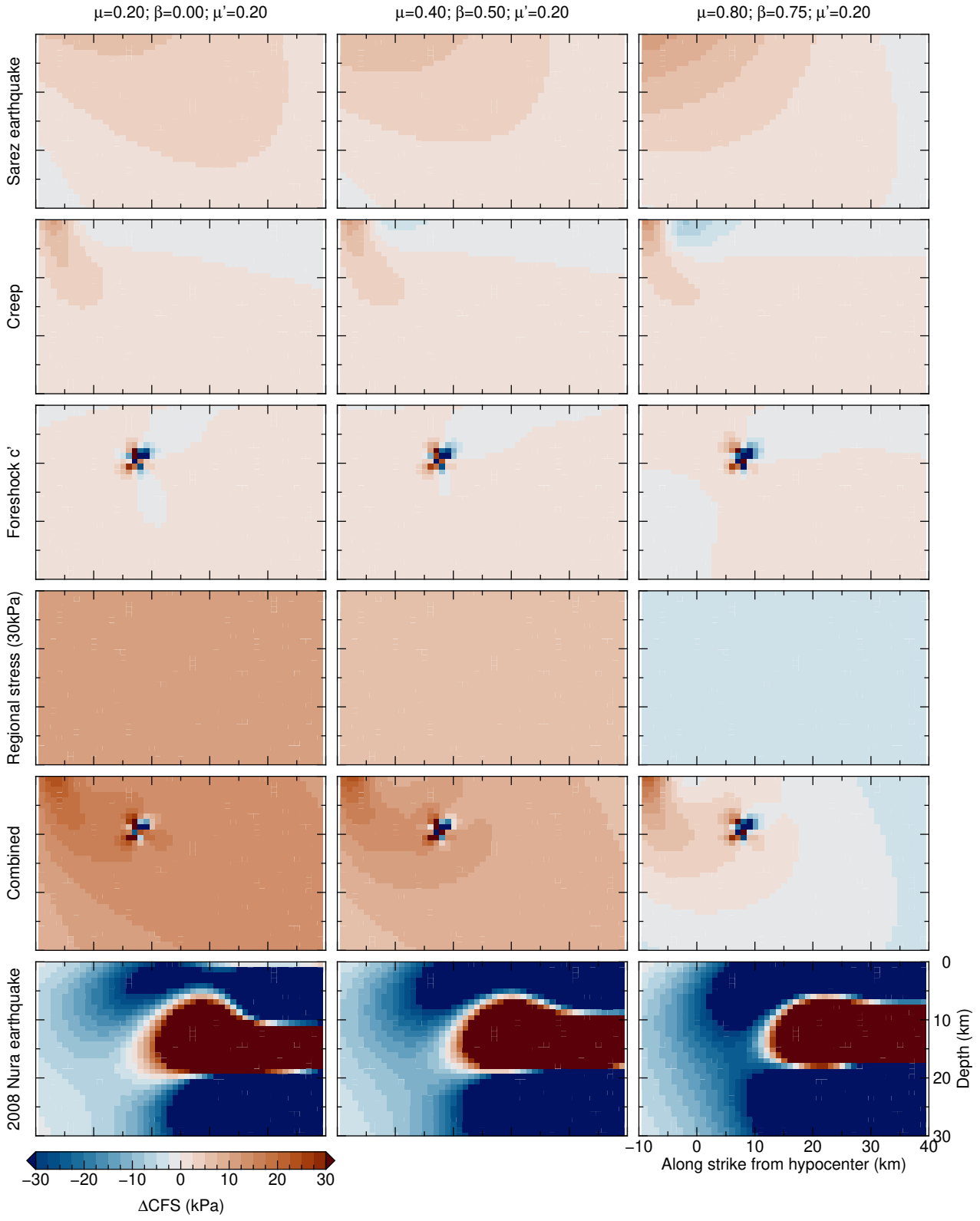

Figure S6. Contributions of distinct stress sources to the change in Coulomb failure stress (ΔCFS) on the fault plane of the Sary-Tash earthquake and in dependence of friction (μ) and Skempton parameter (β) under constant apparent friction (μ').

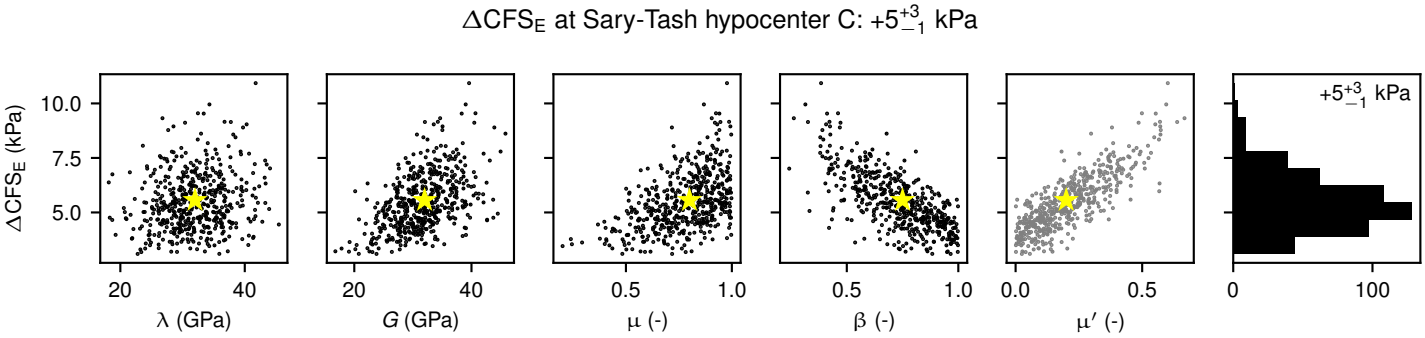

Figure S7. Sensitivity analysis of Coulomb failure stress changes at the Sary-Tash hypocenter *C** due to the Sarez earthquake, postseismic slip on the Sarez fault and foreshock *e'*. Normal distributed Lamé's parameters λ and G, friction coefficient μ, and Skempton's parameter β, with standard deviations of 0.5 GPa, 0.5 GPa, 0.2, and 0.2, respectively, scatter around the preferred values (stars). Derived effective friction μ' shown for comparability. Resulting uncertainty under the assumption of input uncertainties.

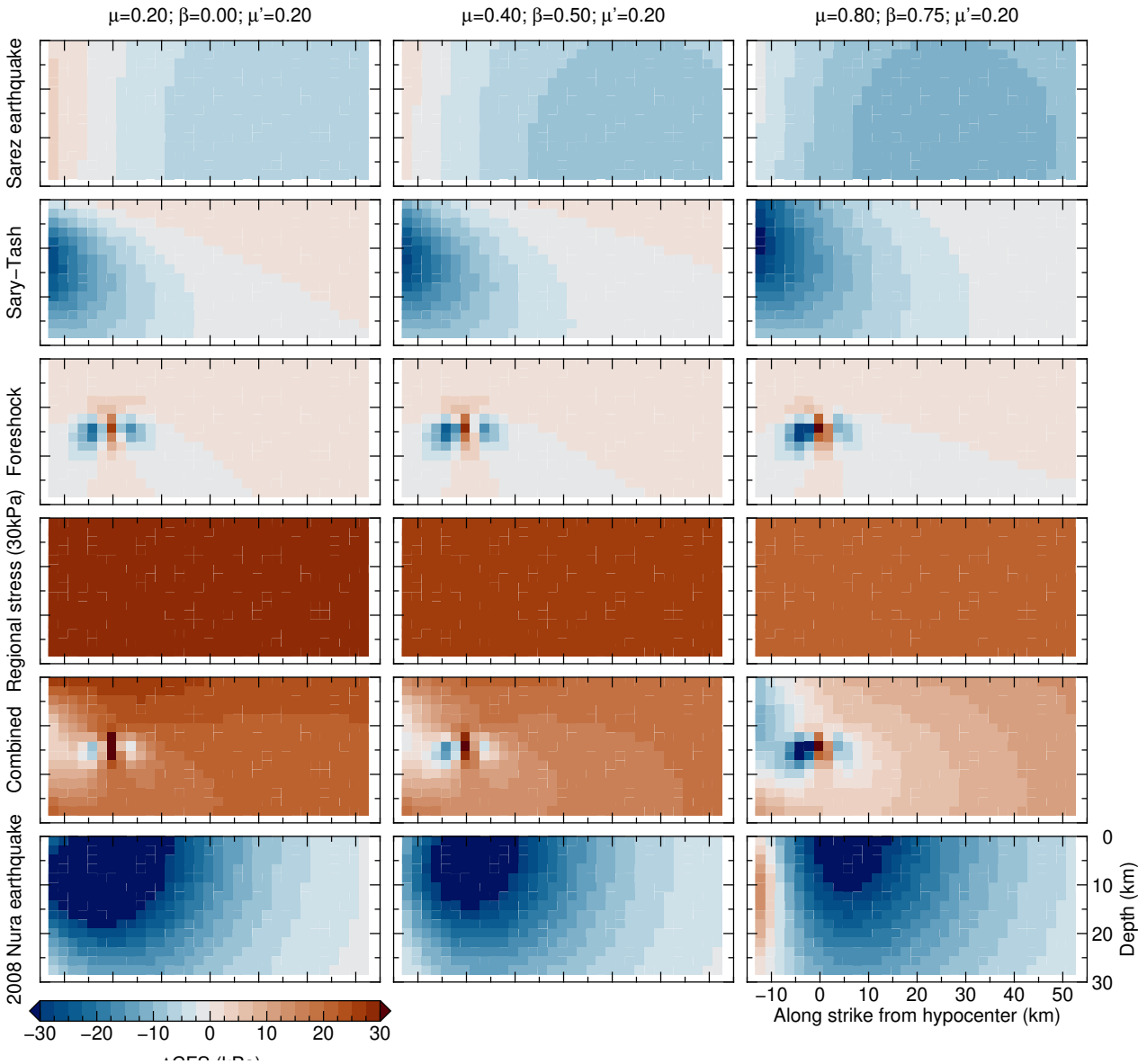

Figure S8. As Fig. S6, but for the Muji earthquake.

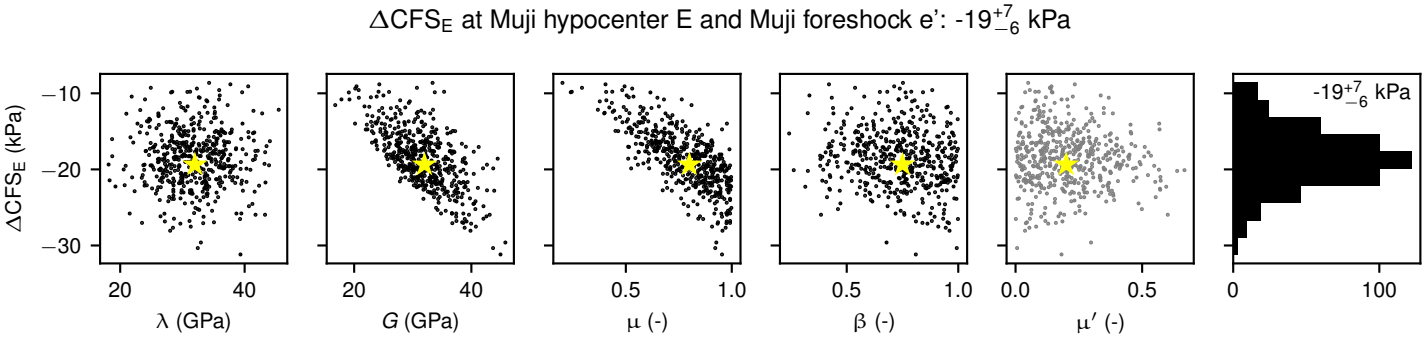

Figure S9. Sensitivity analysis of Coulomb failure stress changes due to the Sarez Sary-Tash earthquakes at the Muji hypocenter *E* and Muji foreshock *e'*, both of which yield the same results within 100 Pa. Abbreviations as in Figure S7.